Tomonaga-Luttinger Liquid Features in Ballistic Single-Walled Carbon Nanotubes: Conductance and Shot Noise

Na Young Kim,* Patrik Recher,† William D. Oliver,‡ and Yoshihisa Yamamoto§
Quantum Entanglement Project, SORST, JST, E. L. Ginzton Laboratory, Stanford University, Stanford, California 94305

Jing Kong¶ and Hongjie Dai
Department of Chemistry, Stanford University, Stanford, California 94305

(Dated: October 5, 2006)

We study the electrical transport properties of well-contacted ballistic single-walled carbon nanotubes in a three-terminal configuration at low temperatures. We observe signatures of strong electron-electron interactions: the conductance exhibits bias-voltage-dependent amplitudes of quantum interference oscillation, and both the current noise and Fano factor manifest bias-voltage-dependent power-law scalings. We analyze our data within the Tomonaga-Luttinger liquid model using the non-equilibrium Keldysh formalism and find qualitative and quantitative agreement between experiment and theory.

PACS numbers: 73.23.Ad, 72.15.Nj, 73.40.Cg, 73.63.Fg

Single-walled carbon nanotubes (SWNTs) continue to provide numerous experimental and theoretical opportunities to investigate one-dimensional physics upon their unique chemical, mechanical, optical and electronic properties [1]. Electrical transport measurements with SWNTs have probed remarkable electronic properties primarily via conductance. The ideal conductance of SWNTs is $2G_{\rm Q} = 2(2e^2/h)$ due to spin and orbital degeneracy in principle, where e is the elementary charge and h is Planck's constant; however, the measured conductance is influenced by the quality of the contacts between a tube and electrodes. For SWNTs weakly coupled to their electron reservoirs (the tunnelling regime), the conductance exhibits a power-law dependence on the drain-source voltage and/or temperature as an indication of a Tomonaga-Luttinger liquid (TLL) [2, 3]. In contrast, Peça *et al.* theoretically analyzed SWNTs strongly coupled to the electron reservoirs (the ohmic regime), claiming that the differential conductance versus the drain-source bias voltage and the gate voltage would unveil traits of the spin-charge separation [4]. Recent theoretical efforts have sought to extend the TLL analysis of ohmic SWNTs to include their current noise properties [5, 6]. Corresponding experimental observations in this regime have remained elusive.

Shot noise, non-equilibrium current fluctuations, originates from the stochastic transport of quantized charged carriers. It probes the second-order temporal correlation of electron current, which often manifests certain microscopic physical mechanisms of the conduction process. When Poisson statistics governs the emission of electrons from a reservoir electrode, the spectral density of the current fluctuations reaches its full shot noise spectral density, $S = 2eI$, where I is the average current. In a mesoscopic conductor, non-equilibrium shot noise occurs due to the random partitioning of electrons by a scatterer, and it may be further modified as a consequence of the quantum statistics and interactions amongst charged carriers [7]. A conventional measure characterizing the shot noise level in mesoscopic conductors is the Fano factor $F \equiv S/2eI$, the ratio of the measured noise power spectral density S to the full shot noise value. Despite growing interest in the shot noise properties of TLLs, current noise measurements in nanotubes have only recently been executed due to the difficulty to achieve highly-transparent (ohmic) contacts and a high signal-to-noise ratio between the weak excess-noise signal and the prevalent background noise [8], although the shot noise properties of SWNTs in the tunnelling regime with no TLL features have been reported [9].

In this letter, we address an experimental and theoretical study of differential conductance and low-frequency shot noise with well-contacted individual SWNTs at liquid ^{4}He temperatures. Experimental results on the differential conductance and low-frequency shot noise reveal clear features of electron-electron interaction. Quantum interference oscillation amplitudes in differential conductance are strongly suppressed at high bias voltages. In addition, the shot noise and the Fano factor exhibit particular power-law scalings with the bias voltage.

SWNT devices have a three-terminal geometry: source, drain, and backgate as illustrated in Fig. 1. The SWNTs were synthesized using an Iron-based Alumina-supported catalyst with a chemical vapor deposition method on a heavily doped Si substrate with a 0.5 μm-thick thermal oxide [10]. The Si substrate was used as the backgate. The metal electrodes were patterned by electron beam lithography, defining the device length. Ti/Au, Ti-only, and Pd metal electrodes were used, which featured low-resistance contacts. Atomic force microscopy imaging enabled us to select devices consisting of a single isolated SWNT with 1.5 $\sim$ 3.5 nm diameter and 200 $\sim$ 600 nm length. We measured the current - gate voltage ($V_{\rm g}$) relation at room temperature in order

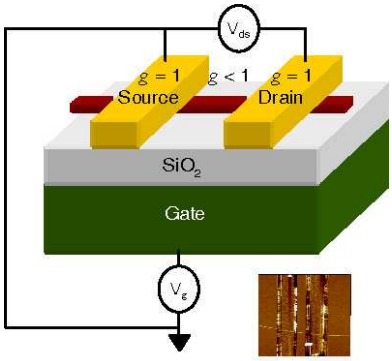

FIG. 1: (Color online) Illustration of a three-terminal SWNT device. The values of the interaction parameter g are indicated in the metal electrodes ($g = 1$) and in the SWNT ($g < 1$). Inset: atomic force microscope image of a device.

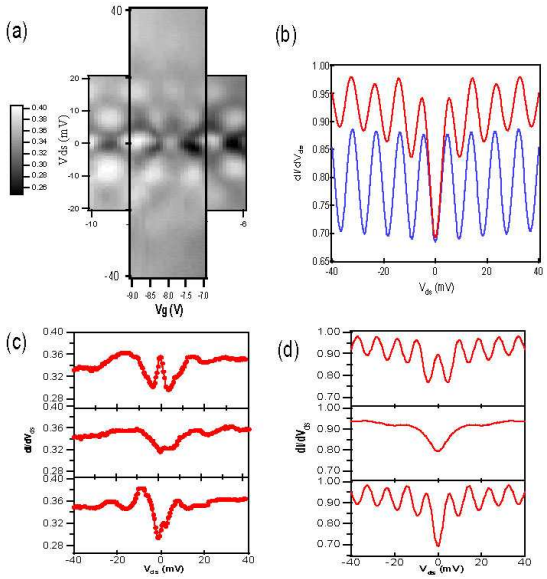

FIG. 2: (Color online) The differential conductance ($dI/dV_{\rm ds}$) graphs in units of $2G_{\rm Q}$. (a) Density plot in the drain-source voltage ($V_{\rm ds}$) and the gate voltage ($V_{\rm g}$). (b) Theoretical $dI/dV_{\rm ds}$ in $V_{\rm ds}$ at a given $V_{\rm g}$ for $g = 1$ (no interaction, blue) and $g = 0.25$ (strong interaction, red) with $U_1 = 0.14$ and $U_2 = 0.1$ at $T = 4$ K. (c) Three experimental traces at $V_{\rm g}$ = - 9 V (top), $V_{\rm g}$= - 8.3 V (middle), and $V_{\rm g}$ = - 7.7 V (bottom). (d) Theoretical traces at $T = 4$ K for U_2 = - 0.1 (top), U_2 = 0 (middle) and $U_2 = 0.1$ (bottom) with $U_1 = 0.14$.

to distinguish metallic from semiconducting tubes. The resistance of selected metallic SWNT devices was typically 12 $\sim$ 50 kΩ at room temperature and about 9 $\sim$ 25 kΩ at 4 K. SWNTs well-contacted to two electrodes with finite reflection coefficients produced a Fabry-Perot (FP) oscillation pattern in differential conductance $dI/dV_{\rm ds}$, ($V_{\rm ds}$ is the drain-source voltage) as an evidence of ballistic transport [11, 12]. Our devices showed the FP interference at low $V_{\rm ds}$, whose diamond structures are caused by the confinement along the longitudinal direction due to the potential barriers at the interfaces with two metal electrodes (Fig. 2(a)). Contrary to the usual FP oscillations, we found in all devices that the interference pattern fringe contrast reduced in magnitude at high $V_{\rm ds}$ as shown in Fig. 2(a). This feature cannot be explained by the standard Fermi liquid (FL) theory, which predicts a constant oscillation amplitude regardless of the bias voltage [11].

Following Ref. [4], we model our device as a TLL with two barriers separating the metal reservoirs from the SWNT and with spatially inhomogeneous interaction parameter g. The interaction is assumed to be strong in the SWNT ($0 < g < 1$) and weak in the higher dimensional metal reservoirs ($g = 1$). The TLL without the barriers is described by the bosonized Hamiltonian [13] $H_{\rm SWNT} = (v_{\rm F}/2\pi)\sum_a \int dx[(\partial_x\phi_a)^2 + g_a^{-2}(x)(\partial_x\theta_a)^2]$, where $\theta_a(x)$ and $\Pi_a(x) = -\partial_x\phi_a/\pi$ are conjugated bosonic variables, i.e. $[\theta_a(x), \Pi_b(x')] = i\delta_{ab}\delta(x - x')$, and $v_{\rm F}$ is the Fermi velocity. The four conducting transverse modes of the SWNT in the FL theory are transformed to four collective excitations in the TLL theory: one interacting collective mode ($a = 1, g_a \equiv g$) of the total charge and three non-interacting collective modes ($a = 2 - 4, g_a = 1$) including spin. These modes are partially reflected at the two barriers. The interacting mode further experiences momentum-conserving reflections due to the mismatch of g at the interfaces [14]. We compute $dI/dV_{\rm ds}$ using the Keldysh formalism and treat the barriers as a weak perturbation. We obtain $I \equiv e(2/\pi)\dot{\theta_1} = 2G_{\rm Q}V_{\rm ds} - I_{\rm B}$ where $I_{\rm B}$ is given to leading order in the backscattering amplitudes as [4, 15]

$$I_{\rm B} = \frac{2e}{\pi t_{\rm F}^2}\sum_{n=1,2} U_{\rm n}\left|\int_0^\infty dt e^{{\rm C_n}(t)}\sin\left(\frac{{\rm R_n}(t)}{2}\right)\sin\left(\frac{eV_{\rm ds}t}{\hbar}\right)\right|, \quad (1)$$

where $t_{\rm F} = L/v_{\rm F}$ is the travelling time for a non-interacting mode along the SWNT length L. The backscattered current $I_{\rm B}$ consists of two contributions: the term proportional to U_1 represents the incoherent sum of backscattering events at the two barriers and the term associated with U_2 results in the FP oscillations due to the coherent interference between backscattering events from different barriers. At high $V_{\rm ds}$, the U_1-term in Eq. (1) dominates and the oscillation amplitude decreases. U_1 and U_2 are independent of $V_{\rm ds}$, but U_2 depends periodically on $V_{\rm g}$ [16]. The interaction parameter g is involved in the time integral through ${\rm C_n}(t)$ and ${\rm R_n}(t)$, which are correlation and retarded functions of the fields θ_a and ϕ_a, respectively. These Green's functions contain a sum over all four collective modes and their forms are obtained at zero [4, 15] and finite temperatures [15].

Figure 2(b) contrasts the effect of electron-electron interaction ($g = 0.25$ (red)) on $dI/dV_{\rm ds}$ with its non-interacting counterpart ($g = 1$ (blue)) for a SWNT of length $L \sim 360$ nm with fitting parameters $U_1 = 0.14$

and $U_2 = 0.1$. The amplitude of the FP oscillation is damped at high $V_{\rm ds}$ compared to that at low $V_{\rm ds}$. Experimental traces show the trend of the FP oscillation amplitude reduction as predicted by the TLL theory for $g = 0.25$; however, the overall conductance of real devices was lower than that in theory. To identify the TLL feature uniquely in experiments requires one to increase $V_{\rm ds}$ above the levelspacing $\hbar/2gt_{\rm F}$. Note that the tendency of amplitude reduction in experimental data cannot be reproduced by the reservoir heating model [17] which asserts that the dissipated power $V_{\rm ds}^2(dI/dV_{\rm ds})$ leads to a bias-voltage dependent electron temperature [18]. We have tested this effect for the non-interacting case ($g = 1$) in our theory and have found that it causes a slight damping of the FP-oscillations (U_2-term) but the incoherent part (U_1-term) is independent of temperature [15]. The temperature effect, therefore, fails to account for the experimentally observed enhanced backscattering amplitude at low $V_{\rm ds}$. In addition, the conductance is relatively small (on the order of G_Q) so that heating effects should not be pronounced in the bias window considered.

Figure 2(c) presents several traces in $V_{\rm ds}$ at different $V_{\rm g}$, from which the following pronounced features are observed: the period of the oscillations at low $V_{\rm ds}$ depends on the value of $V_{\rm g}$, and it becomes elongated at high $V_{\rm ds}$. The former feature can be explained by the TLL model. The model states that the period is $2gt_{\rm F}$ if $U_2 \sim 0$ since the non-zero contribution to the oscillation is only from the interacting mode while the oscillations from the three non-interacting modes destructively interfere [Fig. 2(d)(middle)]. The dominant period is $t_{\rm F}$ produced by the three non-interacting modes when U_2 is maximal (e.g. $U_2 = \mp 0.1$ in Fig. 2(d)(top, bottom)). The $V_{\rm g}$-dependent oscillation periods in $dI/dV_{\rm ds}$ have been interpreted as a signature of spin-charge separation in the SWNT [4]. We find an indication of this effect by comparing the primary periods of these traces, yielding $g \sim 0.22$. The latter feature observed, a longer period at high $V_{\rm ds}$, is beyond our theory, but it is likely to be caused by a strong barrier asymmetry at high $V_{\rm ds}$ which would also suppress the U_2-term. The ratio of primary to elongated periods along $V_{\rm ds}$ gives $g \sim 0.22$ as well. Although compelling evidence, further experiments focusing on the periodicity with $V_{\rm ds}$ should be performed to be conclusive.

The shot noise measurements were performed by placing two current noise sources in parallel: a SWNT device and a full shot noise generator. The full shot noise standard is a weakly coupled light emitting diode (LED) and photodiode (PD) pair. In our 4-K implementation, the overall coupling efficiency from the LED input current to the PD output current was about 0.1 %, which eliminated completely the shot noise squeezing effect due to constant current operation [19]. In order to recover the weak shot noise embedded in the background thermal noise, we implemented an AC modulation lock-in technique and designed a resonant tank-circuit together with a home-built cryogenic low-noise preamplifier [20, 21, 22]. The input-referred voltage noise of the circuit was approximately 2.2 $\rm nV/\sqrt{Hz}$ at 4 K with a resonant frequency $\sim$ 15 MHz. The preamplified signal was fed into a room-temperature amplifier with a gain of about 30 dB, a bandpass filter with low and high cutoff frequencies of 12 and 21.4 MHz, a square-law detector, and a lock-in amplifier. The Fano factor $F(I_i) \equiv S_{\rm SWNT}(I_i)/S_{\rm PD}(I_i)$ was obtained from the ratio of the SWNT current noise spectral density ($S_{\rm SWNT}$) to the LED/PD full shot noise spectral density ($S_{\rm PD}$) at each dc current value I_i. The current noise generated in the LED/PD pair was measured while the SWNT was dc voltage-biased with a constant dc current I_i.

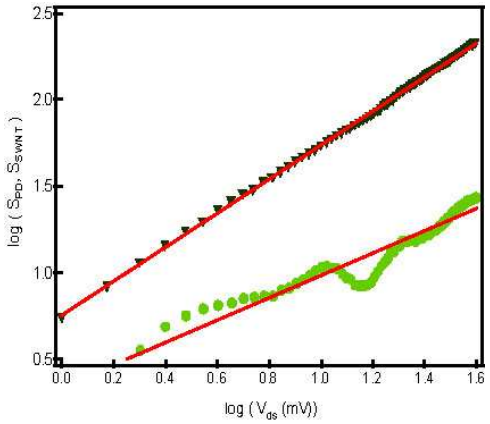

FIG. 3: (Color online) Shot noise power spectral density versus $V_{\rm ds}$ for the LED/PD pair ($S_{\rm PD}$, triangle) and the SWNT ($S_{\rm SWNT}$, dot) at $V_{\rm g}$ = - 7.9 V. The slopes of the shot noise spectral densities are 1 and 0.64 for LED/PD and SWNT respectively, from which the inferred g value for SWNT is 0.16.

Figure 3 shows a typical log-log plot (base 10) of $S_{\rm SWNT}$ in $V_{\rm ds}$ at a particular $V_{\rm g}$. $S_{\rm SWNT}$ (dot) is clearly suppressed to values below full shot noise $S_{\rm PD}$ (triangle), and it suggests that the relevant backscattering for shot noise is indeed weak. Note that $S_{\rm SWNT}$ and $S_{\rm PD}$ have clearly different scaling slopes versus $V_{\rm ds}$.

We extend the theory to calculate the shot noise spectral density, $S_{\rm SWNT}(\omega) = \int dt e^{i\omega t}\langle\{\delta\hat{I}(t), \delta\hat{I}(0)\}\rangle$ with $\delta\hat{I}(t) = \hat{I}(t) - I$ the current fluctuation operator and $\{\cdots\}$ the anticommutator [15]. The SWNT noise in the zero-frequency limit is expressed as $S_{\rm SWNT} = 2e\coth(eV_{\rm ds}/2k_{\rm B}T)I_{\rm B} + 4k_{\rm B}T(dI/dV_{\rm ds} - dI_{\rm B}/dV_{\rm ds})$, becoming $S_{\rm SWNT} = 2eI_{\rm B}$ for $eV_{\rm ds} > k_{\rm B}T$. The asymptotic behavior of $I_{\rm B}$ from the dominant U_1-term when $eV_{\rm ds} > \hbar/2gt_{\rm F}$ follows the power-law scaling $I_{\rm B} \sim V_{\rm ds}^{1+\alpha}$ with $\alpha = -(1/2)(1-g)/(1+g)$. Note that α is uniquely determined by the TLL parameter g. The average value of the power exponent in this sample (Fig. 3) over seven different gate voltages is estimated to be $\alpha \sim -0.31 \pm 0.027$, corresponding to $g \sim 0.25 \pm 0.049$.

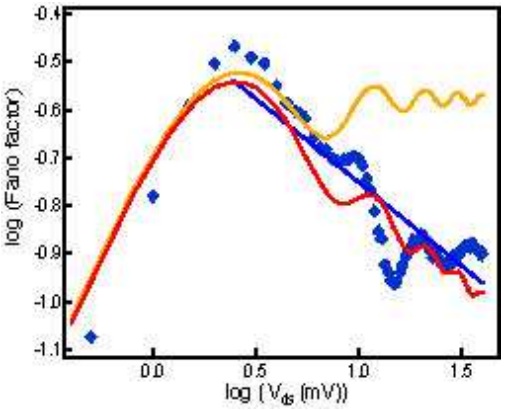

FIG. 4: (Color online) Fano factor versus $V_{\rm ds}$ on a log-log scale. The theoretical Fano factor curves where thermal noise $4k_{\rm B}T\,(dI/dV_{\rm ds})$ is subtracted are drawn for $g = 1$ (yellow) and $g = 0.25$ (red) at T = 4 K with $U_1 = 0.14$ and $U_2 = 0.1$. The power exponent $\alpha \sim$ - 0.35 (blue line) for the measured Fano factor (diamond) at $V_{\rm g}$ = - 7.9 V, and the inferred g value is 0.18. The theoretical $g = 1$ (yellow) plot gives $\alpha \sim 0$ as expected.

The experimental Fano factor $F(I)$ is displayed on a log-log (base 10) scale in Fig. 4. The TLL model predicts that at low bias voltages $eV_{\rm ds} < k_{\rm B}T < \hbar/2gt_{\rm F}$, $F(I) \propto V_{\rm ds}$ after subtracting the thermal noise component $4k_{\rm B}T\,(dI/dV_{\rm ds})$, and its slope is insensitive to g-values in the region of $\log(V_{\rm ds}) < \log(\hbar/2get_{\rm F}) \sim 0.47$ for a 360 nm SWNT and $g = 0.25$ (Fig. 4). On the other hand, if $eV_{\rm ds} > \hbar/2gt_{\rm F}$, a power-law $F \sim V_{\rm ds}^{\alpha}$ is expected by assumption that the backscattered current is smaller than the ideal current $2G_{\rm Q}V_{\rm ds}$. A linear regression analysis of the Fano factor F with $V_{\rm ds}$ in this region, therefore, is another means to obtain the g value. The Fano factors F for $g = 0.25$ (red) and $g = 1$ (yellow) are displayed on a log-log scale in Fig. 4. The experimental data (diamonds) agree well with the theoretical Fano factor of $g = 0.25$. The stiffer slope (α) corresponds to stronger electron-electron interaction. The mean value of the exponent α and the inferred g derived over seven $V_{\rm g}$ values are $\alpha = -0.33 \pm 0.029$ and $g = 0.22 \pm 0.046$ respectively for this particular sample. We find that the measured exponents α and inferred g values from the spectral density $S_{\rm SWNT}$ and the Fano factor F from four different devices with various metal electrodes (Ti/Au, Ti-only, Pd) show similar statistics $\alpha \sim -0.31 \pm 0.047$ and $g \sim 0.26 \pm 0.071$ as derived from several $V_{\rm g}$ values for each sample. We stress that the non-linear decay of the experimental F along $V_{\rm ds}$ indeed starts at a voltage scale $\log(\hbar/2get_{\rm F}) \sim 0.61$ for $g \sim 0.18$ in Fig. 4 as a manifestation of a collective electron effect.

We have measured non-equilibrium differential conductance and shot noise in ballistic SWNTs at low temperatures and analyzed the data within the TLL theory including weak electron backscattering at the SWNT-metal reservoir interfaces. We find convincing agreement between experiment and theory: reduced conductance (FP)-oscillation amplitudes with increasing bias voltage, and power-law characteristics in the weak backscattered current component through low-frequency shot noise measurements. The joint measurement of differential conductance and shot noise provides independent experimental access to the transmitted and backscattered current components of the non-equilibrium transport. This measurement constitutes the first quantitative investigation of TLL interaction effects in the shot noise of SWNTs.

We acknowledge Prof. Quate for his support and atomic force microscopes for imaging the SWNT devices, A. Javey for Pd-contacted devices, and C. Schönenberger, H. Grabert and B. Trauzettel for helpful discussions and comments. This work was supported by the ARO-MURI grant DAAD19-99-1-0215, JST/SORST, NTT, and the University of Tokyo.

* Email: nayoung@stanford.edu
† also at Institute of Industrial Science, University of Tokyo, 4-6-1 Komaba, Meguro-ku, Tokyo 153-8505, Japan
‡ Present address: MIT Lincoln Laboratory, Lexington, Massachusetts, 02420
§ also at National Institute of Informatics, 2-1-2 Hitotsubashi, Chiyoda-ku, Tokyo 101-8430, Japan
¶ Present address: Department of Electrical Engineering, MIT, Massachusetts, 02420

[1] C. Dekker, Physics Today **5**, 22 (1999).
[2] M. Bockrath *et al.*, Nature **397**, 598 (1999).
[3] Z. Yao, H. W. Ch. Postma, L. Balents, and C. Dekker, Nature **402**, 273 (1999).
[4] C. S. Peça, L. Balents, and K. J. Wiese, Phys. Rev. B **68**, 205423 (2003).
[5] B. Trauzettel, I. Safi, F. Dolcini, and H. Grabert, Phys. Rev. Lett. **92**, 226405 (2004); F. Dolcini, B. Trauzettel, I. Safi, and H. Grabert, Phys. Rev. B **71**, 165309 (2005).
[6] A. V. Lebedev, A. Crépieux, and T. Martin, Phys. Rev. B **71**, 075416 (2005).
[7] Y. M. Blanter and M. Büttiker, Phys. Rep. **336**, 1 (2000).
[8] P. -E. Roche *et al.*, Eur. Phys. J. B **28**, 217 (2002).
[9] E. Onac *et al.*, Phys. Rev. Lett. **96**, 026803 (2006).
[10] H. T. Soh *et al.*, Phys. Rev. Lett. **75**, 627 (1999).
[11] W. Liang *et al.*, Nature **411**, 665 (2001).
[12] J. Kong *et al.*, Phys. Rev. Lett. **87**, 106801 (2001).
[13] C. Kane, L. Balents, and M. P. A. Fisher, Phys. Rev. Lett. **79**, 5086 (1997); R. Egger and A. O. Gogolin, Phys. Rev. Lett. **79**, 5082 (1997).
[14] I. Safi and H. J. Schulz, Phys. Rev. B **52**, R17040 (1995).
[15] P. Recher, N. Y. Kim, and Y. Yamamoto, cond-mat/0604613.
[16] We find $U_1 \propto \sum_{ij}[(u_1^{ij})^2 + (u_2^{ij})^2]$ and $U_2 \propto 2\sum_{ij} u_1^{ij}u_2^{ij}\cos(\eta V_g + 2\Delta_{ij})$ where $u_{1,2}^{ij}$ are the bare backscattering amplitudes for barrier 1,2 and between subbands i, j of the SWNT, Δ_{ij} are the corresponding

scattering phases and η is a device-dependent constant.
[17] M. Henny, S. Oberholzer, C. Strunk, and C. Schönenberger, Phys. Rev. B **59**, 2871 (1999).
[18] Heating was proposed as the likely cause for the diminished FP-amplitude with increasing $V_{\rm ds}$ in Ref. [11].
[19] J. Kim and Y. Yamamoto, Phys. Rev. B **55**, 9949 (1997).
[20] M. Reznikov, M. Heiblum, H. Shtrikman, and D. Mahalu, Phys. Rev. Lett. **75**, 3341 (1995).
[21] R. C. Liu, B. Odom, Y. Yamamoto, and S. Tarucha, Nature **391**, 263 (1998).
[22] W. D. Oliver, J. Kim, R. C. Liu, and Y. Yamamoto, Science **284**, 299 (1999).